



Integrated and nonlinear dynamic model of a polymer cable for low-speed cable-driven parallel robots

Sung-Hyun Choi¹ · Kyoung-Su Park¹

Received: 15 November 2017 / Accepted: 25 February 2018 / Published online: 1 March 2018
© Springer-Verlag GmbH Germany, part of Springer Nature 2018

Abstract

Cable-driven parallel robots (CDPRs) have been widely used in various industrial applications requiring high sensitivity. These CDPRs mainly use high strength polymer ropes with light weight and low inertia. However, the polymer cable used in CDPR has the complicated dynamic characteristics such as nonlinear elongation, hysteresis, creep and short and long-term recovery. As CDPR cables are loaded and unloaded under various forces and velocities, dynamic creep and recovery due to loading and unloading strain rate occurs in real time. We proposed the integrated nonlinear dynamic model of polymer cable for the low tensile rate. All of dynamic behaviors were described with only integrated nonlinear dynamic model based on the visco-elastic model. Since the total time when the tension is applied to the system is an important factor in the dynamic creep characteristics, we calculated the loading and unloading time using the concept of equivalent force and the Newton–Raphson method. The constructed model was verified by comparing with experimental results for the hardening effect, dynamic creep, hysteresis and short- and long-term recovery. The proposed model had a good agreement with experimental result.

1 Introduction

Cable-driven parallel robots (CDPRs) find many applications in disaster prevention, construction, testing, and rigging (Williams II et al. 2008; Merlet and Daney 2010; Gobbi et al. 2011). In recent years, such robots have become used in situations requiring high sensitivity (e.g., surgery, and pick-and-place) (Miermeister et al. 2010; Hannaford et al. 2013). Such CDPRs have mainly used lightweight, high-strength polymer ropes with low inertia (Schmidt and Pott 2017). However, unlike steel cables, polymer cables are susceptible to elongation (Chattopadhyay 1997; Cai and Aref 2015), causing positional errors if the nonlinear dynamics of the cables are not considered. Thus, accurate cable modeling is very important in terms of CDPR precision.

Polymer cables used to control CDPRs feature complicated dynamics including nonlinear elongation, hysteresis, creep, and short- and long-term recovery. Many previous

studies have explored cable elongation characteristics. Schmidt and Pott (2017) and Merlet (2009) developed compensation and control algorithms using a modified version of Hooke's law to control the elongation of polymer cables. Miyasaka et al. (2016) developed a hysteresis model. However, previous authors focused on only single simplified characteristics because it is difficult to dynamically model a polymer cable. Such models may be suitable for high-speed systems because the time-dependent effect is small, but are unsuitable for low-speed systems exerting force over a long time, such as the FAST (500 m Aperture Spherical Telescope) with an operating speed of 10 mm/s (Deng et al. 2017). In addition, the hysteresis model of Miyasaka et al. (2016) ignores the creep effect even though that effect dominates cable length deformation. In order that the creep behavior is to be ignored, prior warm-up was required. However, cyclic loading and unloading cause cable cracking, and warm-up process requires a long time to prepare for operation. In real CDPR systems, eight cables are loaded and unloaded under various forces at different velocities. Therefore, dynamic creep and recovery from loading and unloading occurs in real time (Falcone and Ruggles-Wrenn 2009). Dynamic creep is a creep that occurs under a variable force condition rather than a static force condition. For example, when a cable is

✉ Kyoung-Su Park
pks6348@gachon.ac.kr

¹ Department of Mechanical Engineering, Gachon University,
1342 Seongnamdaero, Sujeong-gu, Seongnam-si,
Gyeonggi-do 461-701, Korea

slowly elongated by variable force condition, time-dependent creep may develop because a pseudo-static equivalent force is continuously applied. The time and force-dependence in this situation means dynamic creep. Despite many of these problems, no integrated dynamic model of a polymer cable has yet been established, seriously compromising accuracy.

The existing creep-and-recovery models essentially feature two components: Maxwell model with Hookean spring and Newtonian damper connected in series, and Kelvin Voigt model connected in parallel (Findley and Davis 2013; Augusto et al. 2013). However, the Kelvin–Voigt model does not consider the structural elongation that occurs when loads are applied, and the Maxwell model does not represent the time-dependence of the creep and recovery. To solve these problems, Burger’s model (based on the Maxwell and Kelvin–Voigt models; Li et al. 2000; Chen et al. 2011) has been used in many studies to deal with static creep and recovery characteristics. However, as Burger’s model is a static model, it describes creep and recovery behavior when only static force (not dynamic force) is applied. Therefore, it is necessary to derive the dynamic creep and recovery model dependent on too low tensile rate condition such as FAST. Furthermore, CDPRs have recently been used to manufacture large objects such as three-dimensional printers. The system has the mixed concrete in the end-effector. The mass of mixed concrete is gradually reduced. A continuous slow change in the mass rate can trigger dynamic creep and recovery.

In this paper, we develop an integrated and nonlinear dynamic model of a polymer cable operating at various tensile rates. The model considers dynamic creep, elongation (including the hardening effect), hysteresis, and short- and long-term recoveries. All are introduced via integrated and nonlinear dynamic modeling based on a visco-elastic system. In addition, the Newton–Raphson method is used to obtain loading times under constant tensile rate conditions, and a solution of the dynamic cable model, which is a nonlinear equation, is derived. In the first section, experimental and nonlinear cable dynamics are described. Next, we derive an accurate, theoretical dynamic model for polymer cable. In this section, the static creep (considering the hardening effect) is first derived. Then, dynamic creep and short-term recovery are considered. As loading time is important in terms of dynamic creep, we derive the loading time using the concept of equivalent force and the Newton–Raphson method. Dynamic behavior is predicted using the derived loading time. Next, short- and long-term recoveries are investigated. Long-term recovery is modeled using the Kelvin–Voigt component. Using an integrated dynamics model, we identified the hysteresis behavior. The final model is verified by comparison with experimental data obtained using a tensile test machine and various cable

samples differing in length, tensile strain rate, and applied force.

2 Nonlinear cable dynamics

2.1 Experimental setup

We performed cyclic tensile loading to investigate the creep and hysteresis characteristics of the polymer cable; a Shimadzu AGS-X Plus tensile tester, capable of sustaining forces of up to 20 kN (Fig. 1), was employed. The Dyneema SK78 polyethylene cable used in CDPR systems (that can withstand 2000 N; Weis et al. 2013) was also evaluated. The cable diameter was 3 mm. However, due to the internal configuration of the cable, the diameter changes in a complex manner as force is applied. These changes are too small; thus, in our simulations, we assumed that the cable diameter remained constant. As the system is operated, the cable length changes continuously as the winches wind or unwind the cable. Therefore, we conducted experiments using two cable lengths (100 and 300 mm). Loads of 100–150 N (generally used in CDPR systems) were applied, based on the FALCON cable force (Kawamura et al. 1995). The tensile rates were set at 3 mm/min (Miyasaka et al. 2016) or 50 mm/min to investigate the effects of varying rates. To assess short-term recovery, one loading/unloading cycle was performed. To evaluate long-term recovery, a cyclic loading test using new cable was first performed; then, the tensile test was repeated using the same cable after 24, 48, or 72 h of rest. When measuring long-term recovery, we assumed that the elongation would

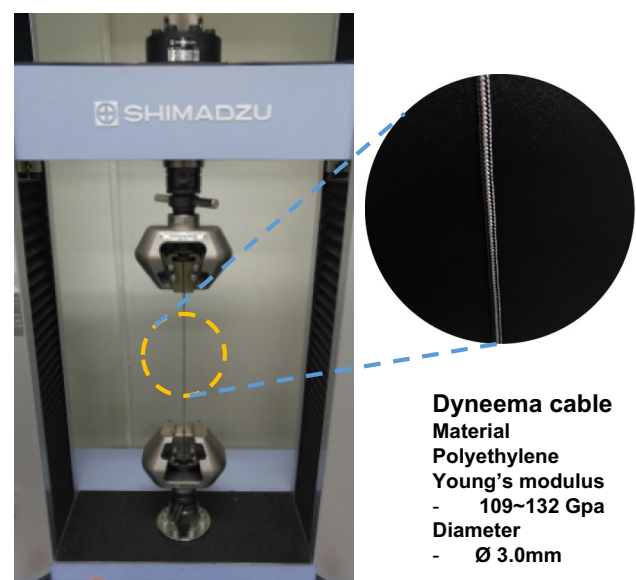


Fig. 1 Experimental setup and cable properties

be the same as the recovery when the same force was applied to the cable in the second tensile test. Finally, recovery was assessed by measuring elongation in the second tensile test. Each experiment was performed three times, and the average values were used in the analysis.

2.2 Nonlinear cable dynamics

Figure 2 shows the qualitative characteristics of the cable during cyclic loading and unloading; the arrows indicate the deformation directions. The red line of left side is the simplest evaluation using a Hooke’s law-based model (static elongation). The green line reflects dynamic behavior when the dynamic creep effect occurs during the red line. It can dominantly occur for case of too low strain rate. In the blue area containing arrow ①, as the cable is slowly elongated, time-dependent dynamic creep occurs because a force equivalent to the constant force is continuously applied. The blue line represents unloading dynamics with consideration of recovery. When 100 N were applied and the load was then returned to 0 N, the length of the cable increased (compared with the initial length). This is because dynamic creep occurred when the cable was stretched. In the yellow area, the cable slowly returns to its original length via short- and long-term recoveries (arrow ②). Note that both creep and recovery are in play during unloading. This means that cable elongation is nonlinear, reflecting both creep and recovery as the cable is unloaded. Also, as loading is repeated, the cable becomes gradually elongated due to dynamic creep and the hardening effect of strain (arrow ③). In contrary, when unloading is maintained, long-term recovery occurs in the cable. Such interactions among creep, recovery, and hardening cause hysteresis. In the Bouc–Wen hysteresis model, not only does hysteresis lack any physical meaning but also constitutes a closed loop (Miyasaka et al. 2016). Thus, the cable length profiles assume discrete values during cyclic loads. This is why the Bouc–Wen hysteresis

model cannot be used to model CDPR cable dynamics. In contrary, the integrated model can be reflect the hysteresis because contains the dynamic behavior for hysteresis. If cyclic loading is repeated, the hysteresis cycles converge because there is no residual dynamic creep. Also, hardening is dependent on strain because hardening reflects physical entanglements of the polymer network that are intensified by deformation (Myung et al. 2007). Thus, hardening also converges as cyclic loading is repeated.

3 A cable model considering the dynamic characteristics

3.1 Static creep and hardening effects

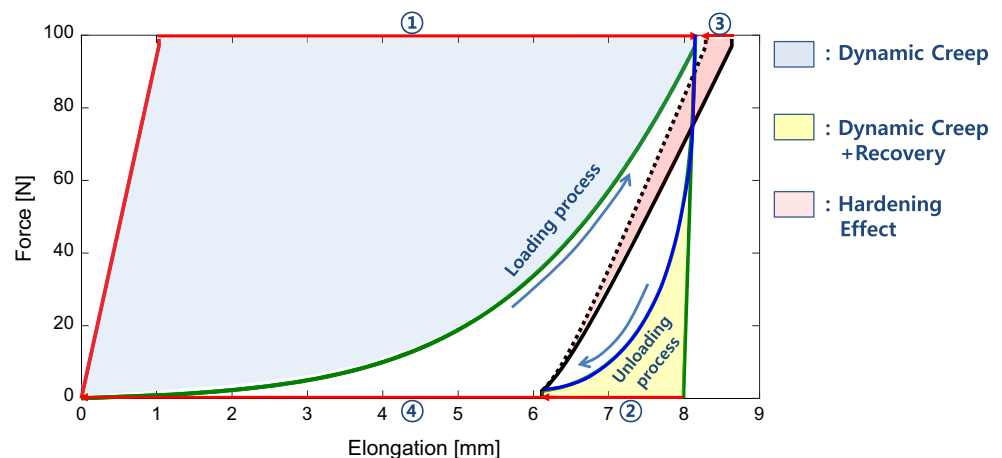
As mentioned above, cable length errors cause control errors; accurate cable modeling is essential. Cable dynamics are affected by cable creep/recovery at all times in CDPR systems. Creep and recovery can be divided into static terms (instantaneous values) and a dynamic term that predominates over time (Lurzhenko et al. 2014). Prior to deriving the dynamic creep, we investigated static effects on the polymer cable. Many previous studies have modeled static creep simply by using the Hookean spring model (Schmidt and Pott 2017; Merlet 2009). However, as loading progresses, hardening caused by develops as modeled below:

$$\epsilon_{c,s} = \left(\frac{F}{E_{1,c}A} \right)^{h(\epsilon_{i-1})} \tag{1}$$

$$h(\epsilon_{i-1}) = 1 + \beta \epsilon_{i-1}^\gamma, \tag{2}$$

where $\epsilon_{c,s}$ is static creep, $E_{1,c}$ is the elastic parameter of static elongation as for the elongation is proportional to the force F . cross-sectional area of the cable is denoted as A , $h(\epsilon_{i-1})$ is the hardening factor the function of total strain at previous step ϵ_{i-1} . β and γ are model parameters. The

Fig. 2 The qualitative characteristics of cable elongation



hardening factor is proportional to residual stress and it corresponds to stretched strain. As a result, it is dependent on the previous strain ε_{i-1} because of the internal structure and polymer network of cable (Myung et al. 2007).

3.2 Time-dependent behavior of cable

In the conventional Burger’s model, the time-dependent creep and recovery are considered only for static forces (i.e. constant forces). The following equations reflect the time-dependent creep and recovery terms of Burger’s model:

$$\varepsilon_c = \frac{F}{E_{2,c}A} \left(1 - e^{-t/t_c}\right) + \frac{Ft}{\eta_0 A} \tag{3}$$

$$\varepsilon_r = \frac{F}{E_{2,r}A} \left(1 - e^{-t/t_r}\right), \tag{4}$$

where $E_{2,c}$ and $E_{2,r}$ are the elastic parameters for time-dependent creep ε_c and recovery ε_r , η_0 is the Newtonian damping parameter following viscous behavior, and t_c and t_r are the creep and recovery retardation times, respectively. The model is dependent on loading and unloading times. During recovery, the damping term connected in series is removed. For static applied tension, Burger’s model as described by Eqs. (3) and (4), has often been used to model polymer creep and recovery properties due to its simplicity. However, this is the static condition based model (Skinner and Rao 1986), which is not suitable for systems where various forces are applied to the cable with too low strain rate. Therefore, the dynamic creep is defined as time-dependent elongation induced by too low strain rate and variable applied tension in this research. First, to derive the loading time, we use a dynamics model based on a visco-elastic model, as follows:

$$\begin{aligned} \varepsilon(t) = & \left(\frac{F_f}{E_{1,c}A}\right)^{h(\varepsilon_{i-1})} - \frac{F_f}{E_{1,r}A} \\ & + \frac{\int_0^{t_{total}} F(t)dt}{t_{total}} \left(\frac{1}{E_{2,c}A} \left(1 - e^{-t_{total}/t_c}\right)\right) \\ & + \frac{1}{\eta_0 A} - \frac{1}{E_{2,r}A} \left(1 - e^{-t_{total}/t_{r,1}}\right) \end{aligned} \tag{5}$$

$$\varepsilon(t) = \int_0^t \dot{\varepsilon}(t)dt \approx \dot{\varepsilon}t_{total} \text{ (For constant strain rate)} \tag{6}$$

where ε is the total strain of cable, $\dot{\varepsilon}$ means the tensile rate of cable, t_{total} means the total time of loading, and F_f is finally applied force. The equation contains creep, recovery, and hardening factors. The integral in the third term of Eq. (5) incorporates the dynamic effect. If the tensile rate is considerably slow, it is regarded as equivalent force at pseudo-static state. Thus, the integral term reflects the equivalent force, and also can be regarded as Eq. (5) equal to Eq. (6) in constant strain rate. Because proposed visco-elastic model has non-linear characteristics with respect to the loading time t_{total} , the actual time was solved using the Newton–Raphson method. The predicted loading and unloading time from the solutions using Eqs. (5) and (6) is for the dynamics behavior.

3.3 Long-term recovery and hysteresis

Another characteristic of cable dynamics is long-term recovery. Piao et al. (2018) solved the long-term recovery problem by adding a Kelvin–Voigt component to Burger’s model. The long-term recovery component is described below:

$$\varepsilon_{r, long} = \frac{\Delta F}{E_{3,r}A} \left(1 - e^{-t/t_{r,2}}\right) \tag{7}$$

$$t_{r,2} = \lambda_1 \left(\frac{1}{\dot{\varepsilon}}\right)^2 - \lambda_2, \tag{8}$$

where $\varepsilon_{r, long}$ is the long-term recovery strain, is dominant at variation of force ΔF from last load F_f , $E_{3,r}$ means the elastic parameter of long time recovery, $t_{r,2}$ means the retardation time of the long-term recovery. It is dependent on the strain rate $\dot{\varepsilon}$, the model parameter of $t_{r,2}$ denoted as λ_1, λ_2 . The polymer cable returns to its original length by long-term recovery as shown in Eq. (7). Such cable properties have been reported by many authors (Van der Werff and Pennings 1991; Hammad et al. 2015). Finally, the dynamics model can be derived by combining previously modeled equations:

$$\varepsilon_i = \begin{cases} \left(\frac{F_f}{E_{1,c}A}\right)^{h(\varepsilon_{i-1})} - \frac{\int_0^{t_{total}} F(t)dt}{t_{total}} \left(\frac{1}{E_{2,c}A} \left(1 - e^{-t_{total}/t_c}\right) + \frac{1}{\eta_0 A}\right) & \text{(Loading)} \\ \left(\frac{F_f}{E_{1,c}A}\right)^{h(\varepsilon_{i-1})} - \frac{F_f}{E_{1,r}A} + \frac{\int_0^{t_{total}} F(t)dt}{t_{total}} \left(\frac{1}{E_{2,c}A} \left(1 - e^{-t_{total}/t_c}\right) + \frac{1}{\eta_0 A} - \frac{1}{E_{2,r}A} \left(1 - e^{-t_{total}/t_{r,1}}\right) - \frac{\Delta F}{E_{3,r}A} \left(1 - e^{-t_{total}/t_{r,2}}\right)\right) & \text{(Unloading)} \end{cases} \tag{9}$$

where the derived loading time t_{total} is again substituted into the proposed visco-elastic model for dynamic behavior [Eq. (9)] to obtain a solution for the dynamic strain. The dynamic creep and recovery effects are modeled using the concept of equivalent force. The first and second terms are instantaneous effects of cable, thus not time-dependent. However, as the hardening effect $h(\varepsilon_{i-1})$ is a function of the strain of the previous step, this should always be modeled together with dynamic creep to derive the strain. Hysteresis is an important dynamic characteristic, caused by a combination of dynamic creep, hardening, and short- and long-term recoveries. Hysteresis develops due to differences in the extent of creep during recovery and changes in stiffness caused by the hardening effect. Our proposed model basically reflects the dynamic behavior of hysteresis, which is why hysteresis was not modeled separately.

4 Verification of the integrated model

To evaluate the proposed model, we performed experiments under linearly increasing stretch and cyclic tensile loads. In cyclic loading tests, 10 loading cycles were applied. Each elongation measured with the 2000 measuring point per cycle (data sampling). Experiments were performed using cables 100 mm and 300 mm in length l , and tensile rates of 3 mm/min and 50 mm/min. The applied forces were 100 N and 150 N. Simulation of short-term recovery featured single-cycle loading at each force for each length of cable. To explore long-term recovery, we performed two tests. The first was a cyclic loading test using new cable under 100 N of force. Then, the tensile test was repeated under the same force after 24, 48, and 72 h of rest. We assumed that if the cable was re-stretched using the same force as in the first experiment, the cable would elongate to the full extent of the recovery. The measured cable elongations were compared with those predicted by the model. Each experiment was performed three times, and the average values calculated. To compare the integrated dynamic model, we used the concept of hysteresis energy dissipation because hysteresis reflects overall dynamic behavior. Each parameter is summarized in Table 1 based on the progressed experiment.

Figure 3 shows the force–elongation profiles at different elongation speed conditions. The tests were performed at constant tensile rates. The force exerted ranged from 0 to 100 N and the cable length was 300 mm. The red and blue lines are the profiles at tensile rates of 50 and 3 mm/min, respectively, and the black dotted lines represent the simulated result by the integrated nonlinear dynamic model of dyneema cable. The errors are measured using the average of the RMS errors by comparing the strain for force. For each condition, the average error was 0.20 mm (3.5%) at

Table 1 Parameters of the creep-and-recovery model

Parameter	Value	Parameter	Value
$E_{1,c}$	1.8 Gpa	$E_{1,r}$	3 Gpa
$E_{2,c}$	8.2 Mpa	$E_{2,r}$	8.0×10^2 Mpa
η_0	5.0×10^3 Gpa	$E_{3,r}$	6.0×10^2 Mpa
t_c	62.5 s	$t_{r,1}$	1 s
β	0.0035	λ_1	8.65×10^5
γ	3.83	λ_2	1.0×10^3
$\dot{\varepsilon}$	3 mm/min, 50 mm/min	A	7.06 mm ²
l	100 mm, 300 mm	F_f	100 N, 150 N

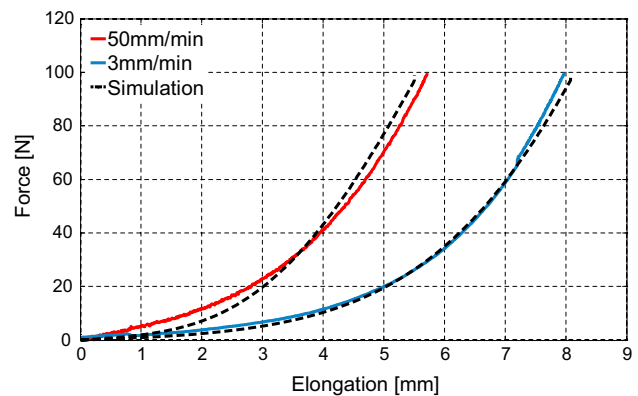


Fig. 3 The effect of tensile rate (tensile rate of 50 and 3 mm/min)

50 mm/min and 0.06 mm (0.72%) at 3 mm/min. The lower tensile rate (3 mm/min) was associated with more elongation over time, as shown in Fig. 3. In other word, as the cable stretches slowly, a time-dependent creep occurs continuously, and the amount of creep is 4 times larger than the static elongation at a tensile rate of 3 mm/min. Because of them, the consideration of tensile rate is essential for the polymer cable. On the other hand, it is less affected by dynamic creep if the cable is tensioned by high tensile rate (50 mm/min). This is because the force is applied for less time than is the case for the lower tensile rate.

Figure 4 shows cyclic loading test result (experimental and simulated). In the simulation, Eqs. (5) and (6) is used to obtain the loading, unloading time, Eq. (9) is used to obtain the elongation history. Since the experiment is not related to long-term recovery, the long-term recovery model is ignored in Eq. (9). The green and red lines are experimental result for a cable under maximum forces of 150 and 100 N, respectively, and the black lines represent the simulations. The experiments were performed at a tensile rate of 3 mm/min. As shown in the graphs, the stiffness increased and converged to one cycle as loading progressed (Schmidt and Pott 2017), due to time-dependent

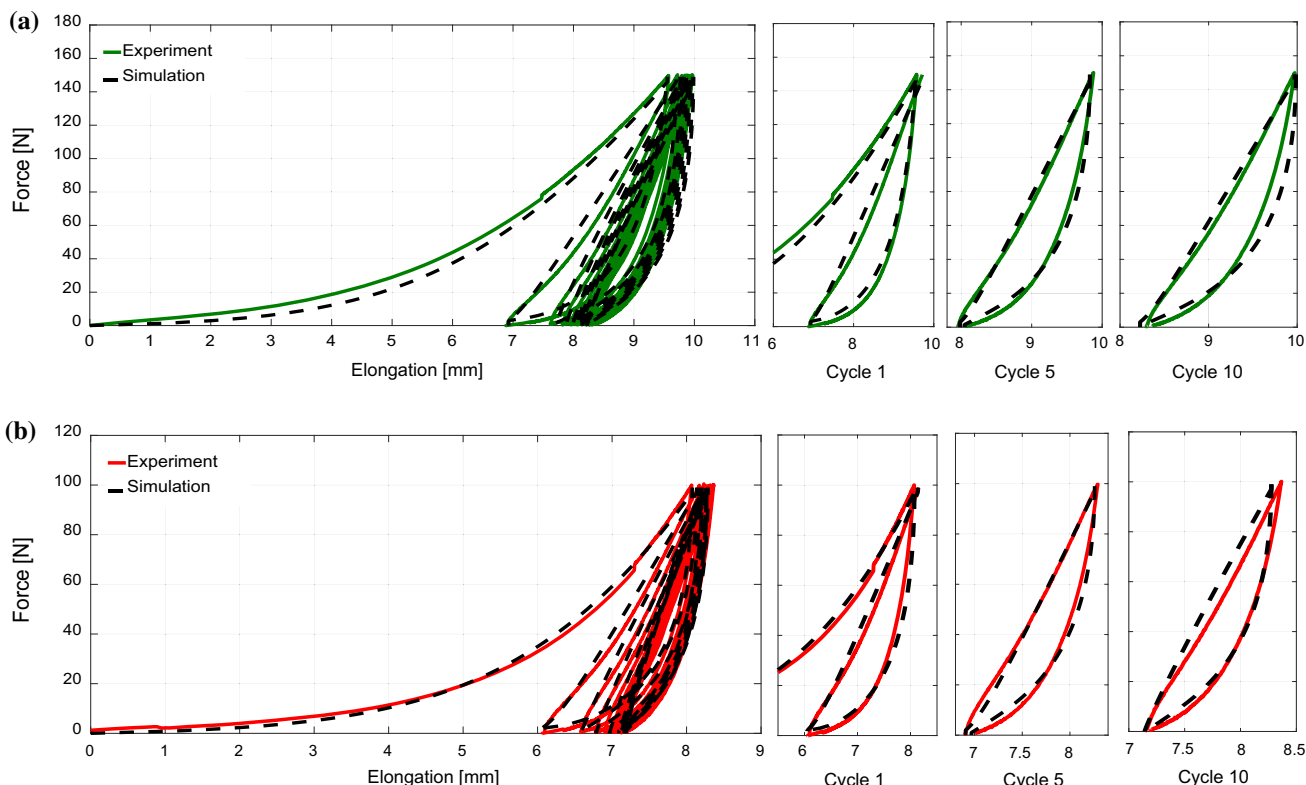


Fig. 4 The cyclic loading test: **a** maximum force of 150 N, **b** maximum force of 100 N

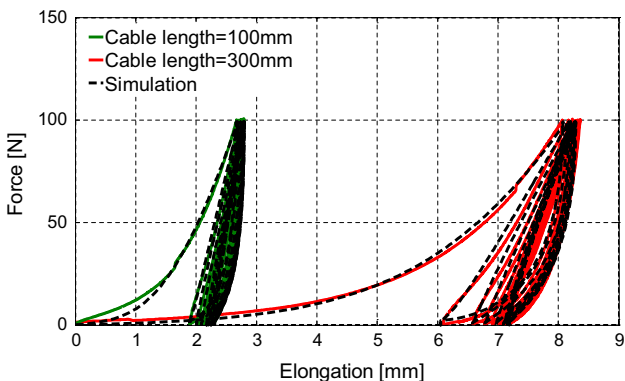


Fig. 5 The Cyclic loading test (cable lengths of 300 and 100 mm)

dynamic creep and hardening as strain is applied to the cable. To measure the error, the difference of average strains for applied force between simulation and experiment result are used. For the two loading conditions, the average errors were 0.03 mm at 100 N and 0.09 mm at 150 N. Each errors are under the 1.6%.

Figure 5 shows cyclic loading test result (experimental and simulated) by cable length. The elongation history was obtained in the same way as in the previous experiment. The green and red lines are the experimental profiles. The maximum applied force was 100 N. The errors are also measured using the average strain for applied force. In the

simulations, the average error in the 100 mm cable length tests was 0.027 mm. The error was thus within 0.9%. However, notably, if the cable length changed under the same loading conditions, elongation was not proportional to cable length. For example, during the time of application of 0 N of force in the first unloading, the 300 mm cable elongated by 6.1 and the 100 mm cable by 1.85 mm. This is explained by the tensile rate. With the 300 mm cable, 3 mm/min is 1%/min but, with the 100 mm cable, 3 mm/min is 3%/min. This affects the cable loading time. Therefore, the time-dependent creep differs. Based on the data of Figs. 4 and 5, when exploring the accuracy of the hardening effect, the averaged gradient was calculated linearly by using the initial force (0 N) and the end force (100 or 150 N). And errors were compared using the each gradients (Fig. 6). Also, cable lengths of 100 mm and 300 mm were used when evaluating the hardening effect (Fig. 7). As the cycles progressed, the stiffness increased via the hardening effect and, then, the increasing rate thereof fell. This is because no residual stress remained as the loading cycle progressed. The errors are in 7.5% compared with experiment.

Figure 8 shows the short-term recovery data for cables of different lengths under various maximum forces. The force trajectory featured a single cycle of loading and unloading. We explored two cable lengths and two

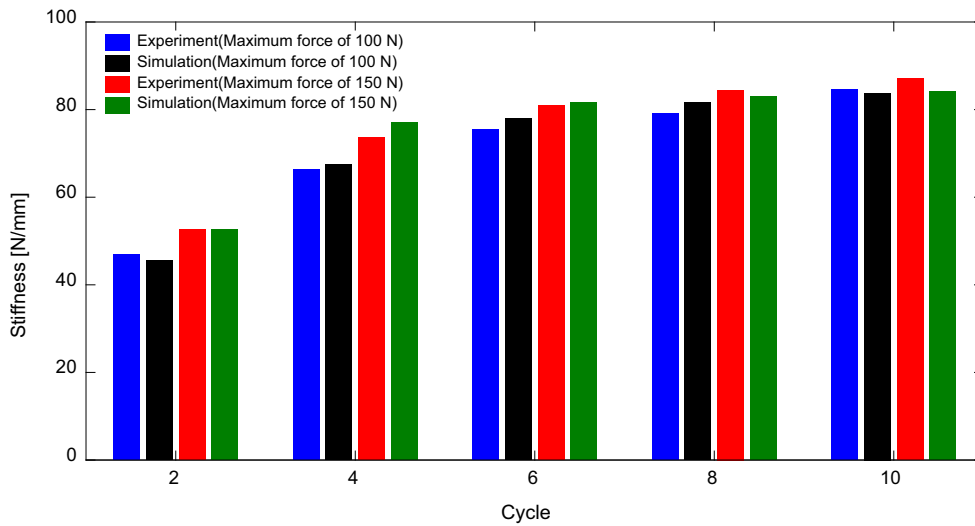


Fig. 6 Stiffness hardening effect by cycle number according to the maximum force (cable length of 300 mm)

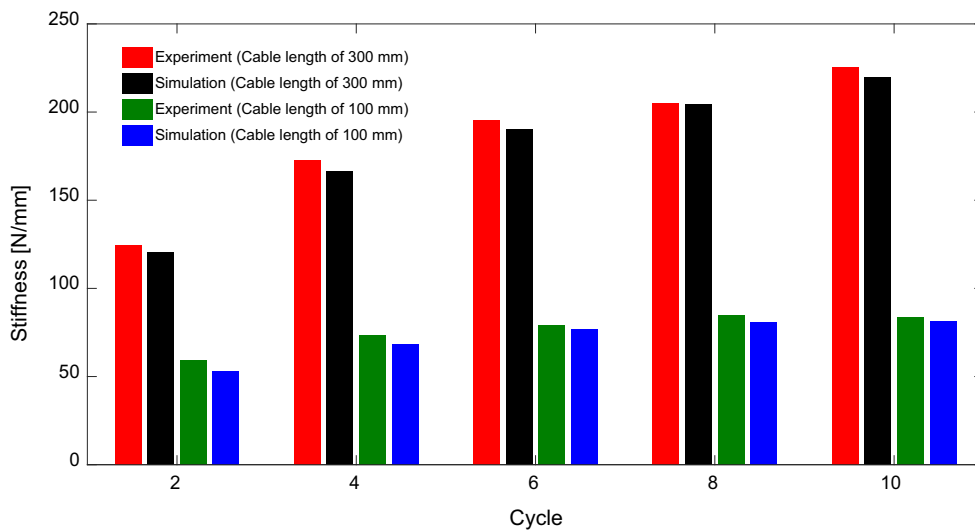


Fig. 7 Stiffness hardening effect by cycle number according to the cable length (maximum force of 100 N)

Fig. 8 The cyclic loading test for short-term recovery (maximum force of 150 N and cable length of 300 mm; 100 N and 300 mm; and 100 N and 100 mm)

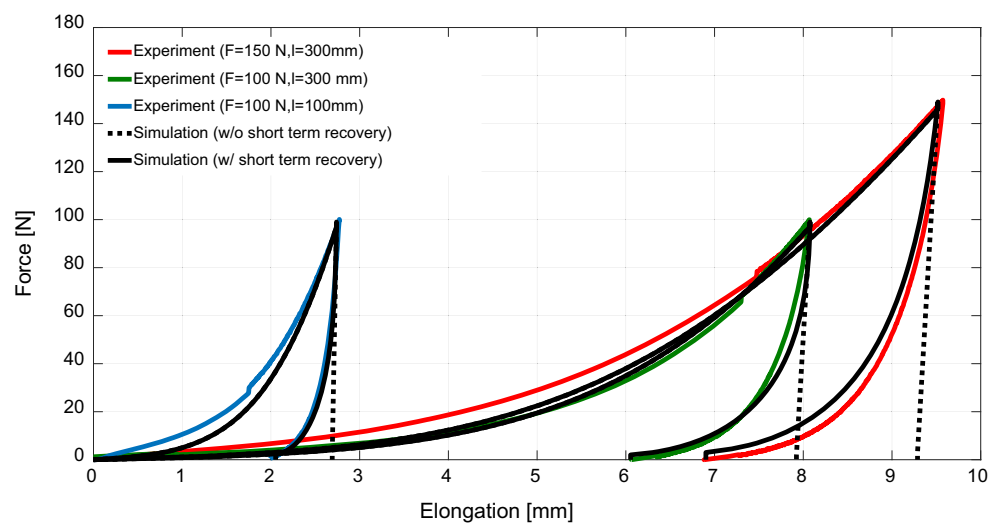
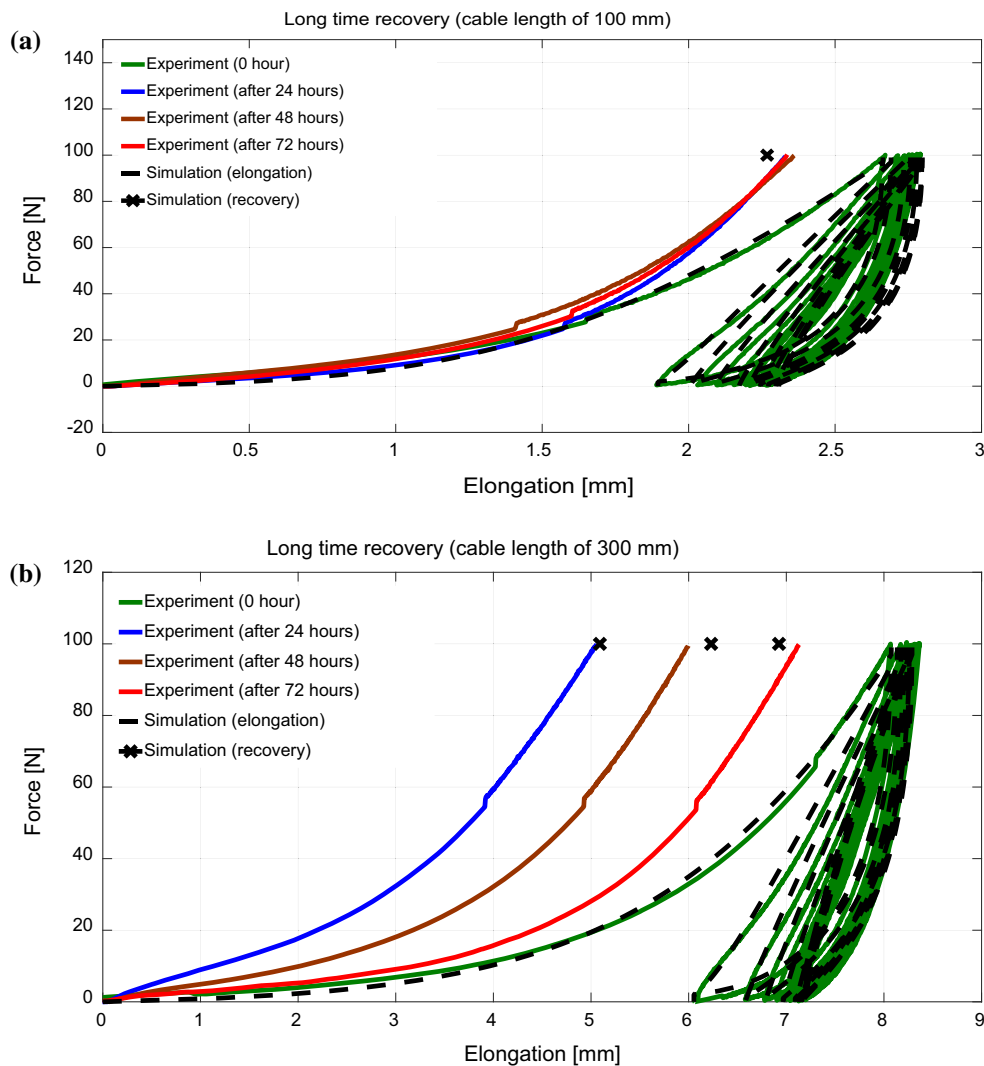


Table 2 Each error of the case without short-term recovery and the case of considering the short-term recovery

	100 N (100 mm)	100 N (300 mm)	150 N (300 mm)
Experimental [mm]	1.99	6.07	6.96
w/o short term recovery [mm]	2.69	7.92	9.28
Error [%]	35.13	30.48	33.33
w/short term recovery [mm]	2.05	6.05	6.90
Error [%]	3.02	3.30	0.86

Fig. 9 The cyclic loading test for long-term recovery: **a** cable length of 100 mm, **b** cable length of 300 mm



maximum forces. The colored lines are experimental data. The red lines are data obtained when the cable length was 300 mm and the maximum force 150 N. The green and blue lines are data obtained under a maximum force of 100 N with cables 300 mm and 100 mm in length, respectively. The black dotted lines are the simulated data without short-term recovery, and the black bolded lines correspond to those with short-term recovery. If such recovery is not considered, the lines are straight at unloading time. However, when short-term recovery is

considered, elongation is nonlinear when unloading and tends to follow the experimental curves because unloading is initially most affected by short-term recovery. The errors (measured at 0 N) are listed in Table 2, and are very low. If short-term recovery is not considered, the errors increase as cyclic loading progresses.

Figure 9 is graph for investigate the long-term recovery of cable. We first used new cable and then repeated the test using the same cable after 24, 48, and 72 h. It is essential that the cable is tested under the same force, because we

Table 3 Each error of the case long-term recovery

	24 h	48 h	72 h
100 mm			
Exp. [mm]	2.33	2.33	2.36
Sim. [mm]	2.26	2.26	2.26
Errors [%]	2.74	2.95	3.90
300 mm			
Exp. [mm]	5.05	5.99	7.12
Sim. [mm]	5.09	6.23	6.92
Errors [%]	0.65	3.90	2.86

assumed that when the same force was applied, the elongation would be the same as the recovery. In the both of graph in Fig. 9, the green lines represent cyclic tensile test data using new cable. The blue, brown, and red lines are tensile test data obtained after 24, 48, and 72 h, respectively. Due to the assumption mentioned above, the black marks reflect long-term recovery. The retardation time of the shorter cable was faster. Compared with the 300 mm cable, the strain rate was relatively high, and, thus, the dynamic creep occurred over less time. Thus, recovery was relatively faster (less dynamic creep). The errors are listed in Table 3.

As mentioned above, hysteresis reflects a combination of cable dynamics. Thus, use of an accurate hysteresis loop

Table 4 Energy dissipation of the hysteresis (Maximum force of 100 and 150 N)

	Cycles	1	2	3	4	5
Hysteresis energy dissipation	100 N					
	Exp. [J]	0.776	0.233	0.192	0.176	0.157
	Sim [J]	0.777	0.226	0.184	0.170	0.150
	150 N					
	Exp. [J]	1.331	0.478	0.395	0.372	0.355
	Sim [J]	1.360	0.450	0.375	0.345	0.340
	Cycle	6	7	8	9	10
Hysteresis energy dissipation	100 N					
	Exp. [J]	0.158	0.154	0.147	0.147	0.144
	Sim [J]	0.149	0.141	0.138	0.138	0.138
	150 N					
	Exp. [J]	0.339	0.327	0.320	0.316	0.305
	Sim [J]	0.331	0.327	0.322	0.322	0.320

Table 5 Energy dissipation of the hysteresis (Cable length of 100 and 300 mm)

	Cycle	1	2	3	4	5
Hysteresis energy dissipation	100 mm					
	Exp. [J]	0.258	0.094	0.084	0.078	0.073
	Sim [J]	0.250	0.092	0.084	0.076	0.070
	300 mm					
	Exp. [J]	0.776	0.233	0.192	0.176	0.157
	Sim [J]	0.777	0.226	0.184	0.170	0.150
	Cycle	6	7	8	9	10
Hysteresis energy dissipation	100 mm					
	Exp. [J]	0.071	0.068	0.065	0.065	0.064
	Sim [J]	0.067	0.063	0.061	0.060	0.059
	300 mm					
	Exp. [J]	0.158	0.154	0.147	0.147	0.144
	Sim [J]	0.149	0.141	0.138	0.138	0.138

controls the accuracy of the integrated model when cyclic loading tests are performed. When comparing hysteresis response, energy dissipations (i.e., the areas of hysteresis) are generally used (Wolons et al. 1998; Amini et al. 2015). Tables 4 and 5 compare hysteresis energy dissipation with respect to the maximum force applied and the cable length. Nonlinear decreasing trends are evident in all cases as the cycles progress. This is because dynamic creep decreases over subsequent cycles. In all simulations, the average and hysteresis errors of the cable dynamics were < 5%. Such results further emphasize that our proposed approach based on visco-elastic model affords reasonably accurate modeling of cable dynamics.

5 Conclusions

Here, we develop an integrated dynamics cable model using creep, short- and long-term recoveries, the hardening effect, and hysteresis to accurately predict CDPР cable lengths. However, Burger's model, which has often been used previously, is not suitable for modeling dynamic CDPР operations, as the model considers only the static state. Therefore, we created an advanced model integrating dynamic behavior using a modified visco-elastic model. In addition, based on force history, the Newton–Raphson method was used to predict the loading time. Simulations were performed under different maximum forces, with different cable lengths, and applying various tensile rates. The simulations were compared with experimental data. During verification, we focused on hardening effects, dynamic creep, short- and long-term recoveries, and hysteresis. We first tested the effect of constant tensile rate; this affected dynamic creep. In the test, a high tensile rate was associated with less dynamic creep than a low tensile rate. We also performed cyclic loading to evaluate dynamic cable behavior and hardening. We found that hardening and dynamic creep changed as cyclic loading progressed. Because of hardening and dynamic creep, the stiffness was increased and then converged as the loading cycle was progressed. Also, the hysteresis loops converged. All simulation errors were < 5%. In contrary to creep, the recovery was occurred when the cable was unloaded. The recovery was divided to short- and long-term recovery. Each recovery occurred in real time and interacted with creep. In particular, consideration of short-term recovery when the cable was unloaded remarkably reduced length errors. For long-term recovery, the retardation time decreased as the cable length was reduced. The new model was highly accurate under various resting conditions and when using cables of different lengths. Finally, we explored hysteresis, which integrates dynamic features including creep, hardening, and long- and short-term

recoveries. The simulated hysteresis and experimental hysteresis were in good agreement. Errors in cable length were remarkably reduced using the proposed model. Thus, some features of the model are essential to improve the accuracy of cable positioning in CDPРs, and the kinematics of CDPР systems depend on cable length.

Acknowledgements This research was supported by Leading Foreign Research Institute Recruitment Program through the National Research Foundation of Korea (NRF) funded by the Ministry of Science and ICT (MSIT) (2012K1A4A3026740) and by Development of Space Core Technology Program through the National Research Foundation of Korea (NRF) funded by the Ministry of Science, ICT and Future Planning (2017M1A3A3A02016340).

References

- Amini A, Yang C, Cheng C, Naebe M, Xiang Y (2015) Nanoscale variation in energy dissipation in austenitic shape memory alloys in ultimate loading cycles. *J Intell Mater Syst Struct* 26:2411–2417
- Augusto PED, Ibarz A, Cristianini M (2013) Effect of high pressure homogenization (HPH) on the rheological properties of tomato juice: Creep and recovery behaviours. *Food Res Int* 54:169–176
- Cai H, Aref AJ (2015) On the design and optimization of hybrid carbon fiber reinforced polymer-steel cable system for cable-stayed bridges. *Compos B Eng* 68:146–152
- Chattopadhyay R (1997) Textile rope—a review. *Indian J Fibre Text Res* 11:360–368
- Chen YC, Chen LW, Lu WH (2011) Power loss characteristics of a sensing element based on a polymer optical fiber under cyclic tensile elongation. *Sensors* 11:8741–8750
- Deng S, Yang G, Liang Z (2017) Research on astronomical trajectory planning algorithm for FAST. In: 29th Chinese control and decision conference (CCDC), pp 5060–5065
- Falcone CM, Ruggles-Wrenn MB (2009) Rate dependence and short-term creep behavior of a thermoset polymer at elevated temperature. *J Press Vessel Technol* 131:011403–011411
- Findley WN, Davis FA (2013) Creep and relaxation of nonlinear viscoelastic materials. Courier corporation, North-holland
- Gobbi M, Mastinu G, Prevati G (2011) A method for measuring the inertia properties of rigid bodies. *Mech Syst Signal Process* 25:305–308
- Hammad A, Swinburne TD, Hasan H, Del Rosso S, Iannucci L, Sutton AP (2015) Theory of the deformation of aligned polyethylene. In: proceedings of royal society A, p. 20150171
- Hannaford B, Rosen J, Friedman DW, King H, Roan P, Cheng L, Glozman D, Ma J, Kosari SN, White L (2013) Raven-II: an open platform for surgical robotics research. *IEEE Trans Biomed Eng* 60:954–959
- Kawamura S, Choe W, Tanaka S, and Pandian SR (1995) Development of an ultrahigh speed robot FALCON using wire drive system. In: IEEE International conference on robotics and automation, pp 1764–1850
- Li F, Larock RC, Otaigbe JU (2000) Fish oil thermosetting polymers: creep and recovery behavior. *Polymer* 41:4849–4862
- Lurzhenko M, Mamunya Y, Boiteux G, Lebedev E (2014) Creep/stress relaxation of novel hybrid organic-inorganic polymer systems synthesized by joint polymerization of organic and inorganic oligomer. *Macromol Symp* 341:51–56
- Merlet JP (2009) Analysis of wire elasticity for wire-driven parallel robots. In: proceedings of EUCOMES, vol 8, pp 471–478

- Merlet JP, Daney D (2010) A portable, modular parallel wire crane for rescue operations. In: Robotics and automation (ICRA) and IEEE international conference, pp 2834–2839
- Miermeister P, Pott A, Verl A (2010) Dynamic modeling and hardware-in-the-loop simulation for the cable-driven parallel robot IPANema. In: Robotics (ISR), 41st International symposium, 6th german conference on robotics (ROBOTIK), pp 1–8
- Miyasaka M, Haghhighipناه M, Li Y, Hannaford B (2016) Hysteresis model of longitudinally loaded cable for cable driven robots and identification of the parameters. In: IEEE international conference on robotics and automation (ICRA), pp 4015–4057
- Myung D, Koh W, Ko J, Hu Y, Carrasco M, Noolandi J, Christopher N, Curtis W (2007) Biomimetic strain hardening in interpenetrating polymer network hydrogels. *Polymer* 48:5376–5387
- Piao J, Jin X, Choi E, Park JO, Kim CS, Jung J (2018) A polymer cable creep modeling for a cable-driven parallel robot in a heavy payload/application. In: Cable-Driven parallel robot, Springer, Cham pp. 62–72
- Schmidt VL, Pott A (2017) Increase of position accuracy for cable-driven parallel robots using a model for elongation of plastic fiber ropes. *N Trends Mech Mach Sci* 43:335–343
- Skinner GE, Rao VNM (1986) Linear viscoelastic behavior of frankfurters. *J Texture Stud* 17:421–432
- Van der Werff H, Pennings AJ (1991) Tensile deformation of high strength and high modulus polyethylene fibers. *Colloid Polym Sci* 269:747–763
- Weis JC, Ernst B, Wehking KH (2013) Use of high strength fibre ropes in multi-rope kinematic robot systems. *Cable Driven Parallel Robots Mech Mach Sci* 12:185–199
- Williams II RL, Xin M, Bosscher P (2008) Contour-crafting-cartesian-cable robot system concepts: Workspace and Stiffness Comparisons. In: ASME 2008 international design engineering technical conferences and computers and information in engineering conference, pp 3–6
- Wolons D, Gandhi F, Malovhr B (1998) Experimental investigation of the pseudoelastic hysteresis damping characteristics of shape memory alloy wires. *J Intell Mater Syst Struct* 9:116–126